

23 Solid immersion based on ZnSe-for visualization of defects inside diamonds

© N.A. Smirnov^{1,*}, A.O. Levchenko¹, S.V. Kuznetsov², A.B. Egorov¹, V.V. Shutov¹, P.A. Danilov¹, A.A. Nastulyavichus¹, S.I. Kudryashov¹, A.A. Ionin¹

¹ Lebedev Physical Institute, Russian Academy of Sciences, 119991 Moscow, Russia

² LLC „Mikrolaser“, 121205 Moscow, Russia

e-mail: cna1992@mail.ru

Received October 20, 2022

Revised December 29, 2022

Accepted January 20, 2023

Using high-temperature lamellar deformation in an argon atmosphere, diamond samples were sealed into an immersion solid-state composition based on ZnSe to visualize the internal structure of diamond in the visible region of the spectrum. The absence of pyrohydrolysis processes at the ZnSe-diamond interface was shown by the following methods: Raman scattering of light, X-ray phase analysis, scanning electron microscopy with energy dispersive analysis. Visualization of graphic images inside the diamond through a five-millimeter layer of solid-state immersion based on ZnSe was made.

Keywords: ZnSe, solid-state immersion, Raman spectroscopy, diamond immersion.

DOI: 10.61011/EOS.2023.02.55792.7-23

1. Introduction

Diamond is a mineral with unique physical and chemical functionality, while a high refraction index makes it extremely attractive for jewelry applications [1–3]. Internal structure visualization of rough diamonds is essential for detection and localization of defects. This allows to select the best cutting size and shape for future jewelry. Internal structure visualization of a rough diamond is hindered by the presence of faces, due to which high refraction index ($n = 2.4$) at the air–diamond interface results in strong light beam refraction.

Currently, several techniques have been offered in order to solve this problem which include tight contact with a substance with high refraction index [4] or provision of immersion medium with the same refraction index around the diamond. Immersion liquids, fusible glasses and crystalline substances are used as immersion media. The use of immersion liquids is impossible, since even the most high-refractive-index liquids have much lower refraction indices than the diamond (CH_2I_2 ($n = 1.74$), $\text{C}_6\text{H}_5\text{AsI}_2$ ($n = 1.85$), $(\text{Se}_2\text{Br}_2$ ($n = 2.1$)) [5,6] and they are toxic and expensive. The use of As_2S_3 –I–Br [7] and Ge_7Se_9 [8] type fusible chalcogenide glasses is a good alternative to liquids since they have high variation of compositions with refraction indices suitable to diamond and easily surround the diamond immersed in liquid glass [8]. The disadvantages of such glasses include their low radiation resistance and visualization in the near IR spectrum, rather than in the visible spectrum. One of the best materials is zinc selenide (ZnSe) because it has a high refrac-

tion index (≈ 2.4 – 2.6 in 500–1100 nm region)) [9,10], transparency in wide spectral area (0.5– $21\ \mu\text{m}$) and high radiation resistance [11–13]. Two types of immersion layer production around the diamond: hot compaction of ZnSe powder with diamond or deep plastic deformation of the ZnSe/diamond initial optical blank at high temperature. Powder technique is extremely complicated in terms of technical implementation and requires the use of powders with certain grain size, prepared particle surface free of micro impurities. Severe high-temperature plastic deformation of the ZnSe optical blank with a diamond placed between chalcogenide specimens results in tight diamond indentation and is a simpler technique. By now, no information about procedure for production of immersion composites of this class are available in literature, conditions for diamond indentation in ZnSe are not known.

As a result, the purpose of the study was to develop a technique of ZnSe-diamond immersion composite production and to visualize graphical images in the diamond through the ZnSe immersion layer. A polished diamond with images applied inside it was used to test the technique, because it could neutralize optical interface issues and verify the immersion layer production method.

2. Experimental

For initial immersion layer specimens, ZnSe plates with two polished sides and dimensions $15 \times 15 \times 5$ mm were used, typical visible and near IR transmittance spectrum was shown in Figure 1, *a*. For test specimens, powder

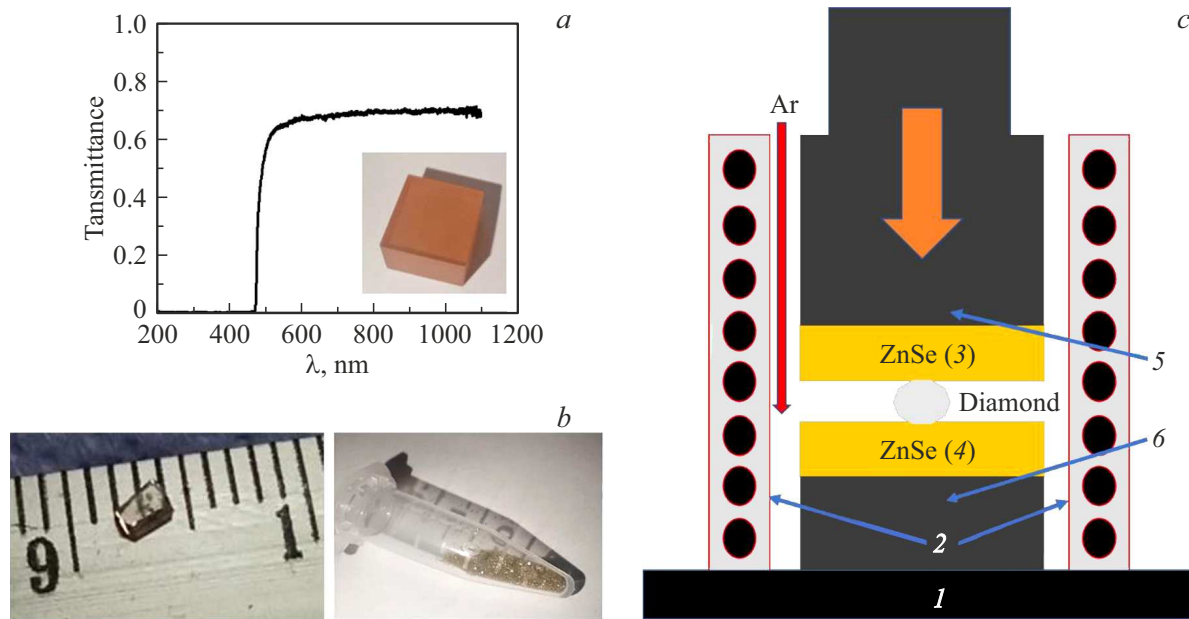


Figure 1. (a) Transmittance spectrum and photo of ZnSe initial immersion plate. (b) Diamond specimens photo. (c) Laboratory bench diagram: 1 — support; 2 — heater; 3, 4 — punches, 5, 6 — press.

containing micro diamonds with a size about $250\mu\text{m}$ and a polished diamond specimen (type IaB) (R_a — 5 nm) in the form of $\sim 2.5 \times 1.5$ mm irregular-shaped plate was used (Figure 1, b). On the surface and inside this diamond, graphical images in the form of lines were applied in advance. The images contained graphitized areas produced using direct laser-beam recording [14–16] with 1030 nm femtosecond emission (0.3 ps) through the lens with numerical aperture $NA = 0.25$. These lines have a length of about $\approx 200\mu\text{m}$ and a width of 10–30 μm . These structures will play a role of defects that will be visualized using optical spectroscopy and Raman scattering spectroscopy.

During development of the laboratory bench for extensive high-temperature plastic deformation, possibility of zinc selenide specimen pyrohydrolysis was taken into account [17,18]. Therefore, protective inert gas purging was carried out — 4.8 grade argon, whose density is higher than air density. The laboratory bench layout diagram is shown in Figure 1, c. The diamond specimen was placed on the ZnSe plate (4) located on the lower punch (6), then the specimen was covered by the second ZnSe plate (3) and tightly secured by the upper punch (5). Before the start of heating, argon flow system was turned on to prevent pyrohydrolysis and heating up to 700°C . When the process temperature was achieved, a force of 10 bar was applied to the upper punch during 30 min followed by cooling down to room temperature. After achievement of room temperature, argon flow was interrupted.

X-ray diffraction analysis of specimens was performed using Bruker D8 diffractometer with $\text{CuK}\alpha$ -radiation. Crystal lattice parameters were calculated in TOPAS software.

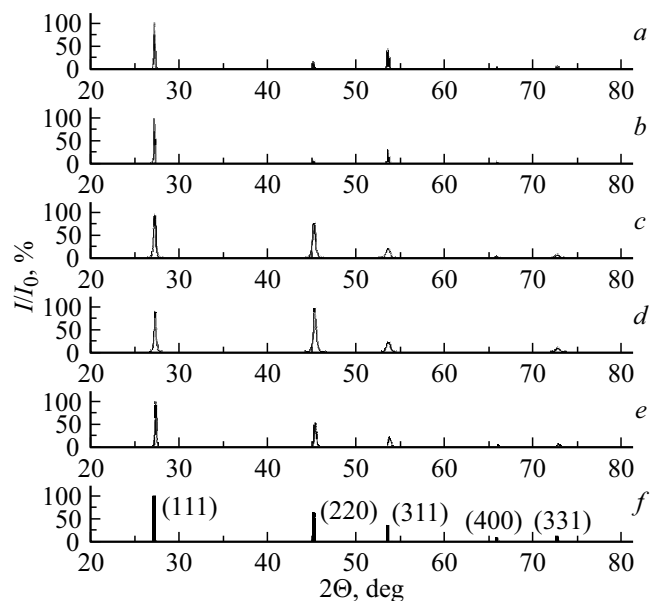


Figure 2. X-ray diffraction analysis of ZnSe specimens: (a, b) initial specimens before pressing, (c) specimen periphery after pressing, (d) specimen center after pressing, (e) powdered specimen after pressing, (f) X-ray database card for ZnSe (JCPDS 00-037-1463). Miller indices are shown in red in brackets.

Scanning electron microscope with energy-dispersive analysis was carried out using TESCAN VEGA IV microscope with Xplore 15 EDX-detector. Optical microscopy was carried out using Altamya MET 5 microscope combined with PC. Raman scattering spectra were recorded by Confotec 350 MR spectrometer with pump laser at 532 nm.

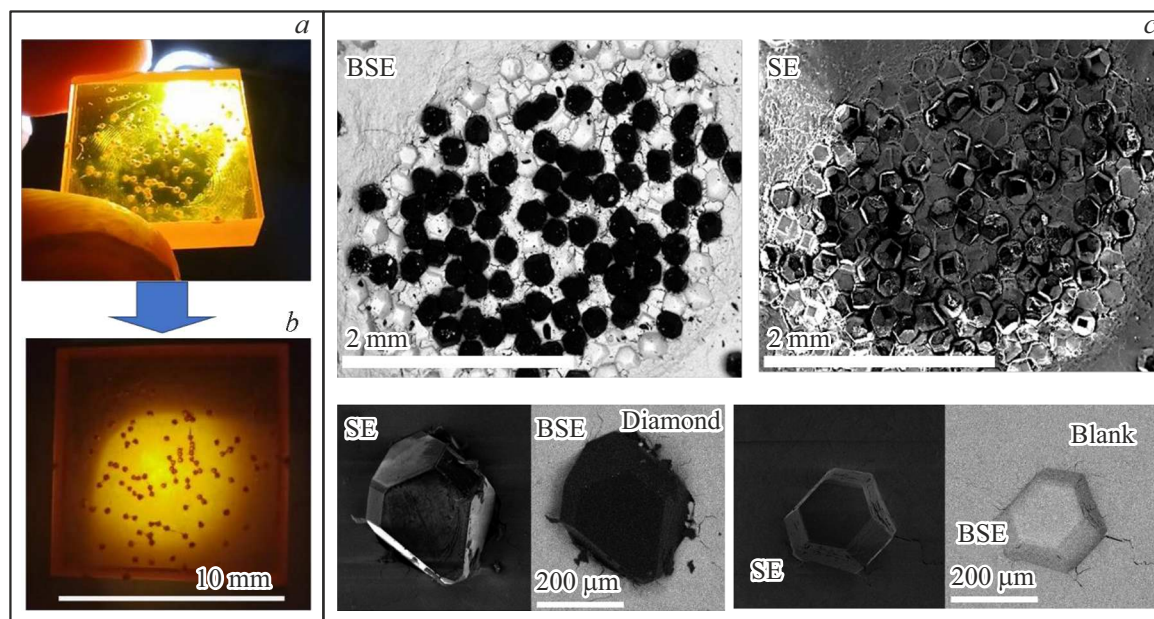


Figure 3. (a) Specimen – General view. (b) Light tested specimen. (c) Visualization of the interface of two ZnSe plates after separation by scanning electron microscope.

Lattice constant calculations

Description	a , Å
Initial specimen 1	5.6687(1)
Initial specimen 2	5.6686(1)
Specimen after the experiment	5.6708(1)
Specimen after the experiment, center	5.6708(1)
Powder after the experiment	5.6697(1)
ZnSe, JCPDS 00-037-1463	5.669

3. Findings and discussion

The first experimental stage included phase composition test of ZnSe plates before and after high-pressure pressing to avoid pyrohydrolysis. X-ray images (Figure 2) of initial and pressed specimens and of the powder produced by partial grinding of the pressed specimens show a similar X-ray pattern, no additional peaks were detected, which agrees with the data on the crystal lattice constant contained in the X-ray database for ZnSe (JCPDS 00-037-1463). Lattice constant calculations for two ZnSe initial plates (Figure 2, *a, b*), specimens after pressing on periphery (Figure 2, *c*) and in the center (Figure 2, *d*) and powdered specimen (Figure 2, *e*) are summarized in the table.

This indicates the absence of pyrohydrolysis processes during deep plastic deformation processes, because the crystal lattice constant has not changed in any significant way. The absence of pyrohydrolysis processes means that the diamond–ZnSe interface will be free from additional phase with unwanted refraction index preventing defect visualization inside the diamond.

For solid state immersion technique, micro diamonds were pressed into ZnSe. Micro diamonds were placed between two ZnSe plates and subjected to high-temperature deep plastic deformation. After completion of the process, ZnSe plates were separated (Figure 3, *a, b*). The general view photos (Figure 3, *a*) and light test geometry (Figure 3, *b*) show that the micro diamonds have been successfully pressed into ZnSe plates. The study of ZnSe surface with pressed micro diamonds by electronic microscopy methods is shown in Figure 3, *c*. For visualization, BSE detector (backscattered electron detector) and SE detector (secondary electron detector) were used. For BSE image, black color corresponds to the diamond and grey color relates to ZnSe. Micro diamonds are tightly pressed into ZnSe. Indentations in ZnSe after mechanical extraction of the micro diamond were examined. The microscopy images show that the micro diamond left a clear and smooth indentation inside ZnSe. No additional colors in BSE mode were detected, which in general indicates that micro diamond pressing into ZnSe is successful without formation of additional phases or micro discontinuities at the materials interface.

In case of chemical analysis using EDX (energy dispersive X-ray spectroscopy) at the micro diamond–ZnSe interface, redistribution of chemical elements was not available (Figure 4, *a*). Also, to confirm the absence of new compounds, Raman scattering spectra (RS) were obtained from micro regions on ZnSe before and after treatment in the area near the micro diamond (Figure 4, *b*). Peaks with centers near 116, 138, 206, 252 and 498 cm^{-1} are observed on the spectra. Peaks near 206, 252 and 498 cm^{-1} are assigned to TO-, 1LO and

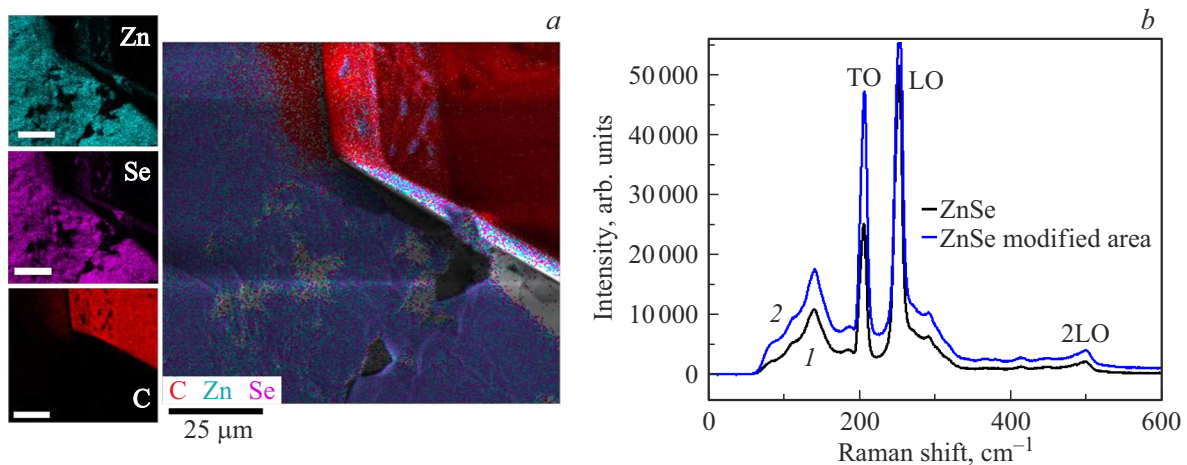


Figure 4. (a) EDX-analysis at the micro diamond — ZnSe interface. (b) Raman scattering spectra of initial ZnSe plate (1) and after pressing near the micro diamond (2).

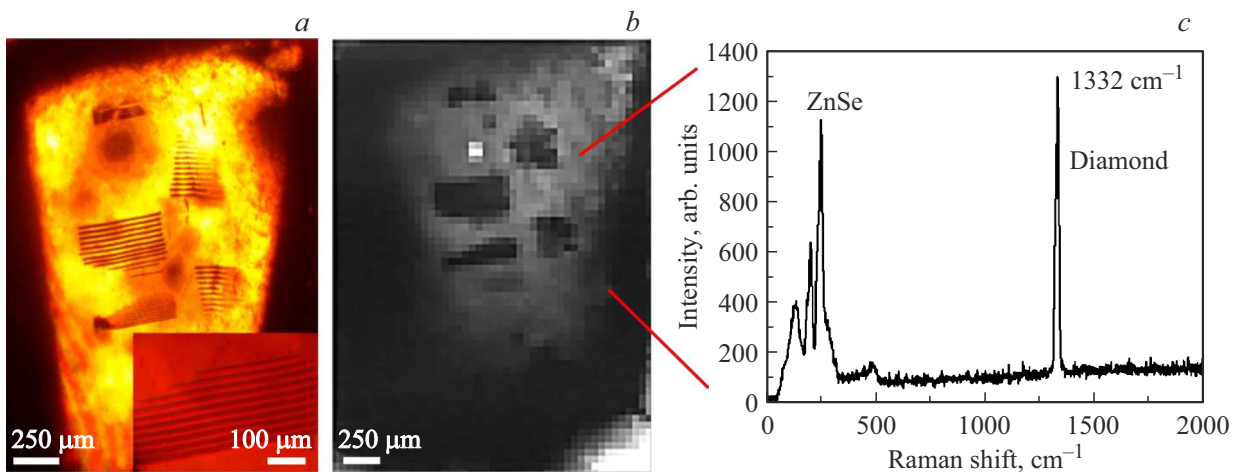


Figure 5. (a) Optical microscope image. Detail (magnified image); (b) Raman scattering map drawn for 1332 cm⁻¹; (c) typical diamond spectrum.

2LO-phonon modes of ZnSe. Peak near 116 cm⁻¹ may be assigned to selenium, while peak near 138 cm⁻¹ may be associated with grain interfaces [19,20]. Insignificant redistribution of peak intensity may be attributed to ZnSe annealing and due to minor stresses occurring in ZnSe [21]. Raman scattering spectra of ZnSe before and after high-temperature plastic deformation change a little, which indicates that there are no phase and structural changes.

Pressing of 2.5 × 1.5 mm diamond into the ZnSe matrix was carried out in a similar way. After diamond pressing into the immersion material, the opposite side of ZnSe was polished. The graphical images in the diamond were visualized through a 5 mm ZnSe-based solid state immersion layer by optical microscopy via a lens with numerical aperture NA = 0.25. Clear graphical images without distortions are observed. There are individual lines obtained using a femtosecond laser, which were recorded

in the diamond before pressing (Figure 5, a). For the main Raman scattering peak of the diamond (1332 cm⁻¹) [22–24] with interval 50 μm, 2D signal strength map was drawn (Figure 5, b). The map shows the diamond plate boundary and layout of graphical images in the diamond, which is represented by a slight decrease of Raman scattering signal (darker regions). For this, it should be noted that all main vibrational peaks of ZnSe are located in the frequency region lower than 500 cm⁻¹ and do not overlap with RS-signal from the diamond (Figure 5, c), which allows to visualize the internal structure of the diamond.

Among other things, ZnSe is a transparent material in the near and middle IR region, which allows to characterize rough diamonds using IR spectroscopy [11–13]. This enhances the use of various spectrum wavelength ranges and equipment for characterization and visualization of micro and macro defects inside diamonds.

Conclusion

By means of high-temperature plastic deformation in argon flow, micro and macro diamonds were successfully pressed into ZnSe to implement the solid state immersion concept. X-ray diffraction analysis, scanning electron microscopy with energy-dispersive analysis and Raman scattering methods demonstrated the absence of pyrohydrolysis processes at the ZnSe-diamond interface. Graphical images inside the diamond were successfully visualized through a 5 mm ZnSe solid state immersion layer.

Acknowledgments

The study was supported by RSF grant 21-79-30063.

Conflict of interest

The authors declare that they have no conflict of interest.

References

- [1] C.J. Wort, R.S. Balmer. *Materials today*, **11** (1–2), 22–28 (2008). DOI: 10.1016/S1369-7021(07)70349-8
- [2] K.V. Ravi. *Materials Science and Engineering. B*, **19** (3), 203–227 (1993). DOI: 10.1016/0921-5107(93)90190-X
- [3] N.Yang, J.S. Foord, X. Jiang. *Carbon*, **99**, 90–110 (2016). DOI: 10.1016/S1369-7021(07)70349-8
- [4] V. Yurgens, J.A. Zuber, S. Flågan, M. De Luca, B.J. Shields, I. Zardo, T. Jakubczyk et al. *ACS Photonics*, **8** (6), 1726–1734 (2021). DOI: 10.1021/acsp Photonics.1c00274
- [5] R. Meyrowitz. *American Mineralogist: J. Earth and Planetary Materials*, **40** (5–6), 398–409 (1955).
- [6] M. Deetlefs, K.R. Seddon, M. Shara. *New Journal of Chemistry*, **30** (3), 317–326 (2006). DOI: 10.1039/B513451J
- [7] A. Semencha, M.G. Dronova, V. Klinkov, A. Osipov, J. Mistry et al. *Key Engineering Materials*, **822**, 848–855 (2019). DOI: 10.028/www.scientific.net/KEM.822.848
- [8] R.A. Khmel'nitskiy, O.E. Kovalchuk, Y.S. Gulina, A.A. Nas-tulyavichus, G.Y. Kriulina, N.Y. Boldyrev, S.I. Kudryashov, A.O. Levchenko, V.S. Shiryaev. *Diamond and Related Materials*, **128**, 109278 (2022). DOI: 10.1016/j.diamond.2022.109278
- [9] H.H. Li. *J. physical and chemical reference data*, **13** (1), 103–150 (1984). DOI: 10.1063/1.555705
- [10] I.V. Gritsenko, M.S. Kovalev, N.G. Stsepuro, Y.S. Gulina, G.K. Krasin, S.A. Gonchukov, S.I. Kudryashov. *Laser Phys. Lett.*, **19**, 076201 (2022) DOI: 10.1088/1612-202X/ac7136
- [11] N.A. Smirnov, A.E. Rupasov, S.N. Shelygina, A.O. Levchenko, M.S. Savinov, S.I. Kudryashov. *Opt. i spektr.*, **130** (4), (2022). DOI: 10.21883/OS.2022.04.52267.52-21
- [12] H. Garcia, J. Serna, E. Rueda. *OSA Continuum*, **3** (3), 498–504 (2020).
- [13] A. Deneuve, D. Tanner, P.H. Holloway. *Phys. Rev. B.*, **43** (8), 6544 (1991). DOI: 10.1103/PhysRevB.43.6544
- [14] G.K. Krasin, M.S. Kovalev, S.I. Kudryashov, P.A. Danilov, V.P. Martovitskii, I.V. Gritsenko, I.M. Podlesnykh, R.A. Khmel'nitskii, E.V. Kuzmin, Yu.S. Gulina, A.O. Levchenko. *Appl. Surface Science*, **595**, 153549 (2022). DOI: 10.1016/j.apsusc.2022.153549
- [15] S.I. Kudryashov, A.O. Levchenko, P.A. Danilov, N.A. Smirnov, A.A. Rudenko, N.N. Melnik, A.A. Ionin. *Appl. Phys. Lett.*, **115** (7), 073102 (2019). DOI: 10.1063/1.5114630
- [16] V.V. Kononenko, T.V. Kononenko, S.M. Pimenov, M.N. Sinyavskii, V.I. Konov, F. Dausinger. *Quantum Electronics*, **35** (3), 252 (2005). DOI: 10.1070/QE2005v035n03ABEH002900
- [17] G.F. Pinaev, A.I. Murashkevich, V.M. Goryaev. *Izv. AN SSSR. Neorgan. materialy* **12**, (7), 1301–1304 (1976) (in Russian).
- [18] M.P. Kulakov, A.V. Fadeev. *Izv. AN SSSR. Neorgan. materialy*, (in Russian) **19** (3), 347 (1983).
- [19] H. Li, B. Wang, L. Li. *J. alloys and compounds*, **506** (1), 327–330 (2010). DOI: 10.1016/j.jallcom.2010.06.201
- [20] E. Mosquera, N. Carvajal, M. Morel, C. Marín. *J. Luminescence*, **192**, 814–817 (2017). DOI: 10.1016/j.jlum.2017.08.017
- [21] C.M. Lin, D.S. Chuu, T.J. Yang, W.C. Chou, J.A. Xu. *Huang. Phys. Rev. B*, **55** (20), 13641 (1997). DOI: 10.1103/PhysRevB.55.13641
- [22] S.A. Solin, A.K. Ramdas. *Raman spectrum of diamond. Phys. Rev. B*, **1** (4), 1687 (1970). DOI: 10.1103/PhysRevB.1.1687
- [23] A. Olejniczak, R. Tomala, P. Zemajtė, A.F. de Araujo Maia, O. Bezkrivnyi, B. Macalik, O. Ignatenko, D. Beben, W. Strek. *Optika i spektr.*, **130** (1), (2022) (in Russian). DOI: 10.21883/os.2022.01.51907.39-21
- [24] E.A. Ekimov, V.A. Sidorov, E.D. Bauer, N.N. Mel'Nik, N.J. Curro, J.D. Thompson, S.M. Stishov. *Nature*, **428**, 542–545 (2004). DOI: 10.1038/nature02449

Translated by E.Ilyinskaya